Distinct structural transitions of chromatin topological domains coordinate hormone-induced gene regulation

François Le Dily[1,2,3], Davide Baù[1,3], Andy Pohl[1,2], Guillermo Vicent[1,2], Daniel Soronellas[1,2], Giancarlo Castellano[1,2,4], François Serra[1,3], Roni H.G. Wright[1,2], Cecilia Ballare[1,2], Guillaume Filion[1,2], Marc A. Marti-Renom[1,3,5,*] and Miguel Beato[1,2,*].

[1] Gene Regulacion, Stem Cells and Cancer Program, Centre de Regulació Genòmica (CRG), Barcelona, Spain

[2] Universitat Pompeu Fabra (UPF), Barcelona, Spain

[3] Genome Biology Group, Centre Nacional d'Anàlisi Genòmica (CNAG), Barcelona, Spain

[4] Hospital Clínic, Universitat de Barcelona, Barcelona, Spain

[5] Institució Catalana de Recerca i Estudis Avançats (ICREA), Barcelona, Spain

***corresponding authors**

Miguel Beato	Marc A. Marti-Renom
E-mail: miguel.beato@crg.es	E-mail: mmarti@pcb.ub.cat
Centre de Regulació Genòmica (CRG)	Centre Nacional d'Anàlisi Genòmica (CNAG)
Dr. Aiguader 88,	Baldiri i Reixac 4,
E-08003, Barcelona, Spain.	E-08028, Barcelona, Spain.
Tel +34 93 316 0119	Tel. +34 934 020 542
Fax +34 93 316 0099	Fax. +34 934 037 279

Keywords: Three-dimensional structure of the genome, gene expression, Hi-C, TADs, transcriptional regulation, epigenetic landscape, progesterone receptor.

Running title: Hormone remodels specialized chromatin domains.

Supplementary Material

Table of contents

1. Supplementary Methods

1.1. Hi-C libraries, reads mapping and filtering and generation of contact matrices.

Hi-C libraries from T47D cells treated or not with the Pg analogue R5020 for 60 min were generated according the previously published Hi-C protocol with minor adaptations (Lieberman-Aiden et al. 2009). Hi-C libraries were performed in both conditions using *HindIII* and *NcoI* restriction enzymes to generate two independent biological and technical replicates. Briefly, cells were fixed with 1% formaldehyde during 10 min at room temperature. Cross-linking reactions were stopped by addition of glycine (0.125 M final). Cells were scraped and nuclei were prepared as described previously. Chromatin digestion, labelling and ligation steps were performed according the original protocol (Lieberman-Aiden et al. 2009). After deproteinisation, removal of biotinylated free-ends and DNA purification, Hi-C libraries were controlled for quality and sequenced on an Illumina Hiseq2000 sequencer. Paired-end reads were processed by first aligning to the reference human genome (GRCh37/hg19) using BWA. Reads filtered from analysis include those that were not uniquely mapped, mapped more than 500 bp from relevant restriction sites, had bad sequence quality (*e.g*. 40% or more of the bases with Sanger PHRED quality ≤ 2) or bad BWA mapping quality (≤ 20), or were located in regions classified to have exceptionally high sequence depth (top 0.1%) by the 1000 Genomes project's data. To offset bias introduced by PCR amplification of the sequencing library, only one of the duplicated pairs were used for subsequent analyses. Datasets normalized for experimental biases and sequencing depth (Lieberman-Aiden et al. 2009) were used to generate contact matrices at 20, 40 and 100 Kb as well as at 1Mb resolutions. The Supplementary table 1 summarizes the number of interactions obtained for each dataset.

1.2. Genome segmentation in TADs.

The genome was segmented in TADs by the TADbit program that includes a change-point algorithm for the detection of TAD borders inspired by methods used to detect copy number variations in CGH experiments (Pique-Regi et al. 2008). Briefly, the optimal segmentation of the chromosome in *k* TADs is computed by maximum likelihood for every *k*, after which a Bayesian Information Criterion selects the best

model. The hypotheses underlying the model are that the number of interactions between two loci has a Poisson distribution, of which the average decreases as a power law function of their separation (in base pairs). Each TAD corresponds to a vertical slice of the Hi-C interaction matrix, where the parameters of the model mentioned above are constant. The TADbit program uses an internal normalization and thus runs on raw interactions. The parameters are corrected for local biases (most notably G+C content, availability of the restriction enzyme site and repeat coverage) (Lieberman-Aiden et al. 2009) that can affect the read count of the bin on column *i* and row *j* by taking the ratio of the sum of reads in column *i* multiplied by the sum of reads in row *j*. The detail of the implementation of TADbit will be further detailed elsewhere (Serra et al., manuscript in preparation).

1.3. Epigenetic data collection and analyses.

MNase-seq, DNase I-seq and ChIP-seq experiments (H3K4me1, H3K4me3, H2A, H4, RNA polymerase II, progesterone receptor, H3K9me3, HP1γ) in T47D cells were described previously (Ballare et al. 2013; Vicent et al. 2013). Additional ChIP-seq experiments for CTCF, H3K36me2, H3K27me3, H3K14ac and H1.2 were performed in similar conditions using the following antibodies: 07-729 (Millipore), 07-369 (Millipore) 39155 (Active Motif), 07-353 (Millipore) and ab4086 (Abcam), respectively. All reads were processed by aligning to the reference human genome (GRCh37/hg19). MNase-seq, DNase I-seq and ChIP-seq signals normalised for sequencing depth were summed in windows of 100 Kb. To generate plots in Supplementary Figures 2 and 3, bins correspond to a fifth of the TAD size (hereafter mentioned as sub-segments). Summed reads for these different window sizes were divided by the corresponding signal obtained for an input DNA of T47D cells to determine the normalised signal over input enrichment/depletion. Progesterone-induced enrichment or depletion of mark content were determined for 100 Kb bins or for the whole TAD as the ratio of sequencing-depth normalised read counts before and after treatment.

1.4. Role of TAD borders in demarking chromatin blocks.

To analyse the role of the TAD borders in limiting epigenetic blocks of individual marks, the opposite of the absolute difference of the signals, normalised as above, was calculated for two consecutive sub-segments (with each TAD divided into 5

segments of equal size) on 3 consecutive TADs. Therefore, the higher the score is, the more similar the signals between consecutive segments. These scores were computed genome-wide, and the quartiles of the 14 consecutive values were calculated to generate the plots in Supplementary Fig. 3a and c. To control that the observed differences were not due to biases in the sizes of the sub-segment, and to confirm the role of the TAD borders, we shuffled the TADs chromosome-wise.

To analyse the homogeneity of epigenetic marks within TADs, we generated pairwise correlation matrices between the profiles of the marks described above for all 100 Kb windows of the genome. From this, we computed the average correlation between 100 Kb windows located in the same TAD. If TADs are homogeneous in chromatin marks combinations, this average correlation will be higher than expected by chance. To estimate the null distribution of this score, we shuffled the TADs chromosome-wise 5,000 times and applied the same procedure. The average correlation obtained with the initial positions of the TADs was higher than the average correlation when the TADs were randomized. Finally, we repeated the same analysis using the differential of the normalised signal after treatment with R5020 and the signal before treatment.

1.5. Expression levels (RNA-seq) and hormone-induced changes.

RNA-seq experiments were performed in T47D treated or not with 10^{-8} M R5020 (Pg) for 1 or 6 h or with 10^{-8} M estradiol (E2) for 6 h. Paired-end reads were mapped with the GEM mRNA Mapping Pipeline (v1.7) (Marco-Sola et al. 2012) using the latest gencode annotation version (v.18) (Harrow et al. 2012). BAM alignment files were obtained and used to generate strand-specific genome-wide normalized profiles with RSeQC (Wang et al. 2012) software. Exon quantifications summarized per gene for expression level determination were obtained either as normalised read counts or reads per kilobase per milion mapped reads (RPKM) using Flux Capacitor (Montgomery et al. 2010). Fold changes (FC) were computed as the $\log_2$ ratio of normalised reads per gene obtained after and before treatment with hormones. To analyse the changes of non-protein coding regions of the genome, the number of normalised reads were computed for chromosomal domains that do not overlap with any annotated protein-coding gene.

In order to compare the observed and expected number of genes positively or negatively affected by hormone treatment and to exclude potential biased responses depending on low/high basal expression of genes, randomizations of protein-coding gene positions used in Figure 2F were obtained as follow: genes were classified in 5 classes of equivalent sizes according their expression level. Gene positions were then shuffled for the 5 classes allowing conserving an equivalent average expression of genes per TAD and therefore avoiding the effect of potential biased distributions frequencies of genes positively or negatively modified depending on the basal levels of expression. Shuffled lists were then used to calculate the percentage of genes with positive or negative fold change per TAD.

1.6. Classification of TAD according transcriptional response to Pg.

To classify TADs according their hormone response, we calculated the average ratio of the number of normalised RNA-seq reads obtained after and before hormone treatment in the RNA-seq replicates. TADs containing more than 3 protein coding genes were saved for further analysis and ranked according to the average ratio described above. The top and bottom 10% were classified as “activated” and “repressed” TADs, respectively.

1.7. Fluorescent in situ hybridization.

T47D cells grown on slides were fixed with 4% paraformaldehyde in PBS 15 min at room temperature. After washes with PBS and permeabilisation with 0.2% Triton X-100 in PBS, slides were incubated 60 min with RNase A in SSC2X. Fixed cells were incubated 3 min in 0.1 N HCl and 1 min in 0.01 N HCl with 0.01% pepsin. Slides were denatured at 70ºC for 8 min in SSC 2×-70% formamide and incubated overnight at 37ºC in a humid chamber with the probes (separately denatured 10 min at 80ºC in hybridization buffer). 100 ng of each probe generated by nick translation using dUTP-biotin, dUTP-DIG and dUTP-fluorescein (Roche Applied Biosciences) was used per hybridization. Detection was performed with ant-biotin-Cy5 (Rockland), anti-DIG-rhodamin (Roche) and anti-fluorescein-Alexa 488 (Invitrogen). Machine optimized stacks were acquired on a Zeiss TCS SP5 confocal microscope. After deconvolution, 3D rendering of the hybridised probes signals were generated for each channel, and

the pair-wise 3D distances between the centre of mass of these signals were computed using the Imaris Software.

The BACs used in this study were obtained from a 32k library:

RP11-758G19	chr1	:	26742822	-	26905278
RP11-443P17	chr1	:	26877973	-	27069024
RP11-973A19	chr1	:	27772963	-	27993702
RP11-667P18	chr1	:	28384701	-	28571122
RP11-318E23	chr1	:	28980912	-	29129694

1.8. Integrative 3D modelling of TADs.

Hi-C data matrices

Hi-C experimental data resulted in interaction counts between the loci of the genomic region of interest (*i.e.* the quantitative determination of the number of times each specific experimental ligation product is sequenced). We then applied an internal normalization by Z-scoring the sequenced raw interaction count data. First, we applied a log2 transformation of the raw counts and then their Z-score was calculated as:

$$Zscore_{ij} = \frac{c_{ij} - m}{s}$$

where μ and σ are the average and standard deviation of the interaction counts for the entire Hi-C matrix. Such normalization allowed us to quantify the variability within the Hi-C matrix as well as to identify pairs of fragments that significantly interacted above or below the average interaction frequency.

TAD representation

Hi-C datasets obtained with *HindIII* and *NcoI* enzymes were pooled to generate normalized Hi-C matrices at 20 Kb resolution. Consequently, each modelled genomic region was represented as a set of particles, one per each 20 Kb bin. Each particle had a radius of 100 nm, based on the relationship of 0.01 nm per base pair (bp)(Harp et al. 2000). Neighbour particles were constrained to lie at an equilibrium distance proportional to the sum of their excluded volume. Non-neighbor particle pairs (*i.e.* particles representing non-consecutive bins along the genomic sequence) were

instead assigned a distance derived from the z-score matrices. The function mapping the z-scores onto distances was defined as the calibration curve built by interpolating the highest and the lowest z-score values, with a minimum proximity distance of 200 nm (the excluded volume of two base particles) and a maximal proximity distance for two non-interacting fragments, respectively, as previously described (Bau and Marti-Renom 2012). The forces applied to the defined restraints were also set proportionally to the absolute value of the Hi-C z-score observed between a pair of fragments.

TAD modelling

Each particle pair was restrained by a series of harmonic oscillator centred on a distance derived from the experimental data. Consecutive particles (*i.e*. particle pairs —or bins— *i, i+1*) were considered as neighbour particles and therefore retrained at an equilibrium distance proportional to the sum of their excluded volume. Non-neighbour particles (*i.e.* particle pairs —or bins— *i, i+2..n*) were instead restrained at distances calculated from a function that mapped their corresponding z-scores onto distances. This function corresponded to a calibration curve that was built between the points defined by the maximum and minimum z-score values, and two empirically determined minimum and maximum distances, respectively. The maximum distance for non-interacting loci was independently optimized for each modelled region (Supplementary Table 2). Consecutive particles were restrained by an upper-bound harmonic oscillator, which ensured that two particles could not get separated beyond a given equilibrium distance proportional to the sum of their excluded volume. Non-consecutive particles were restrained by two different oscillators: (i) an harmonic oscillator, which ensured a pair of particles to lie at about a given equilibrium distance and (ii) lower-bound harmonic oscillator, which ensured that two particles could not get closer than a given equilibrium distance. In both cases the equilibrium distance was derived by a calibration curve defined by the points corresponding to the maximum and minimum z-score values with a minimum and a maximum distance (see below). The different type of oscillator applied depended on an upper (*uZ*) and a lower (*lZ*) z-score cut-off as well as the approximation distance between two non-interacting particles (*aD*), as previously described (Bau and Marti-Renom 2012). The values of *uZ*, *lZ* and *aD* were independently optimized for each modelled region (Supplementary Table 2). Neighbour particles were constrained by an upper-bound

harmonic oscillator centered at an equilibrium distance proportional to the sum of their excluded volume. Non-neighbour particles with a z-score higher than the upper-bound cut-off (*uZ*) were restrained by a harmonic oscillator, while pairs of particles with a z-score lower than the lower-bound cut-off (*lZ*) were restrained by a lower-bound harmonic oscillator. Since these two harmonic oscillator aim at keeping a pair of particles at an equilibrium distance or further apart from a minimal distance, respectively, pairs of non-neighbour particles that were observed to interact with z-scores above the *uZ* parameter were kept close in space, while pairs of non-neighbor particles that were observed to interact with z-scores below the *lZ* parameter were kept apart. The *k* force applied to these restraints was set to the square root of the absolute value of their interacting z-scores. Finally, pairs of non-neighbour particles for which Hi-C data were not available were restrained based on the average z-score of the adjacent particles.

Model building with IMP

Following the steps previously described (Bau and Marti-Renom 2012), we modelled the 3D structure of 61 genomic regions. The selected regions included a total of 209 TADs and covered about 267 Mb of the genome (Supplementary Table 3). Once the system was fully represented and the restraints between the particles were set, IMP generated the ensemble of solutions that best represented the input data by simultaneously minimizing the violations of all the imposed restraints. Due to the large conformational space to be explored and to the population-based nature of 3C-based methods, the optimization of the imposed restraints resulted in different configurations with similar final IMP objective function. Thus, to comprehensively explore the conformational space of the modelled TADs, we generated a large number of models for each conditions (2,000 models for each) by globally minimizing the imposed restraints via a combination of 10,000 Monte Carlo rounds with 5 local steps in a molecular dynamics simulation with a standard simulated annealing method. At each optimization step, the conformation was randomly changed and the change was accepted or rejected according to the Metropolis criteria. The driving scoring function that was minimized during the optimization protocol consisted of the sum of all the individual restraint scores between all the particles representing the system. The entire calculation of 122 independent simulations resulting in 244,000 different conformational solutions (2,000 for each region and hormone treatment),

took about 6 days on a 200 CPU cluster computer.

Model analysis

To further characterize the structural perturbations on TADs by the treatment with Pg, we performed a series of computational analysis in a set of 1,000 selected models with the lowest IMP objective function, which correspond to the 3D models that best satisfy the initial imposed restraints (Bau and Marti-Renom 2012).

The entire set of analysis included:

a) Structural clustering of models.

   To structurally compare two 3D models, we used pair-wise rigid-body superposition minimizing the root mean square deviation between the superposed conformations. The comparison resulted in a 1,000×1,000 symmetric matrix of all-against-all structural comparisons storing the number of particles for every pair of aligned models that align within 75 nm distance cut-off. The comparison matrix was then used as input file to the Markov Cluster Algorithm (MCL) program (Enright et al. 2002), which generated unsupervised sets of clusters of related structures.

b) TAD radius of gyration.

   The radius of gyration of an object (in our case a TAD) is root mean square distance of the objects' parts from its centre of gravity. We calculated for each TAD a centre of gravity and then measured the distance of all points in the TAD to this centre. The average value of the distances corresponded to the TAD radius of gyration. The larger the radius of gyration is, the more open the TAD is.

c) TAD and particle accessibility.

   The particle accessibility of a model is the accessible fraction of its particle to a hypothetical spherical object of a given radius (in our calculations 75 nm). To obtain such fraction, we first build a mesh of points surrounding each particle in the model, which indicates its theoretical occupancy. Then, the spherical object is placed on all possible positions in contact with the model and the fraction of the mesh around the particle that is can be occupied by the object is considered accessible. The accessibility change

for a given TAD was calculated as the ratio of the sums of all particle accessibilities in the TAD before and after Pg.

d) Ensemble visualization

The UCSF Chimera package (Yang et al. 2012), a highly extensible program for interactive visualization of molecular structures, was used to produce all images of the modelled TADs.

2. Supplementary Tables

Supplementary Table 1: Summary statistics Hi-C datasets

	HindIII -Pg	HindIII +Pg	NcoI -Pg	NcoI +Pg
Sequenced Fragments Pairs	189563259	146045810	186633896	232632568
Interacting Fragments Pairs*	74015388	48530773	100262904	120640304
"Intra-chromosomal"	29552177	19519911	49163452	57721468
"Inter-chromosomal"	44463211	29010862	51099452	62918836

*: after mapping and filtering

Supplementary Table 2: IMP optimal modelling parameters

Region	Chrom	Start bin	End Bin	uZ	lZ	aD	CC
1	1	10500	10660	0.0	-0.6	400	0.78
2	1	11315	11590	0.0	-0.3	400	0.75
3	1	1815	1925	0.6	0.0	500	0.77
4	1	3015	3200	0.0	-0.3	400	0.68
5	1	5830	6000	0.3	-0.6	400	0.75
6	1	8375	8575	0.0	-0.3	400	0.74
7	1	9070	9315	0.6	-0.3	500	0.76
8	2	11025	11240	0.0	-0.3	400	0.68
9	2	2105	2290	0.3	-0.3	400	0.76
10	2	3480	4010	0.9	-0.3	500	0.70
11	2	480	660	0.0	0.0	400	0.78
12	2	7910	8045	0.6	-0.3	500	0.71
13	2	9940	10130	0.0	-0.3	500	0.70
14	3	7515	7920	0.9	-0.6	500	0.71
15	3	8395	8500	0.6	0.0	500	0.80
16	4	1970	2100	0.3	0.0	500	0.75
17	4	355	490	0.0	-0.3	500	0.82
18	4	3990	4165	0.0	-0.3	400	0.68
19	4	4410	4760	0.0	-0.6	400	0.63
20	4	5245	5480	0.6	-0.3	500	0.70
21	5	2605	2915	0.0	-0.3	400	0.73
22	5	535	810	0.9	-0.6	500	0.69
23	5	7050	7405	0.9	-0.3	500	0.73
24	6	2680	3200	0.9	-0.3	500	0.72
25	6	3590	3825	0.6	-0.3	500	0.69
26	6	7560	7665	0.9	0.0	600	0.72
27	6	7885	8055	0.0	-0.3	400	0.75
28	7	2410	2740	0.6	-0.6	400	0.69
29	7	4390	4610	0.0	-0.3	500	0.65
30	7	7830	7956	0.3	0.0	500	0.78
31	8	2675	2850	0.0	0.0	500	0.76
32	8	455	595	0.0	-0.3	400	0.75
33	8	5195	5345	0.0	-0.6	400	0.74
34	9	0	105	0.6	0.0	500	0.74
35	9	5855	6240	0.3	-0.6	400	0.70
36	9	6960	7060	0.0	-0.6	500	0.88
37	10	1065	1545	0.6	-0.3	500	0.67

38	10	2595	2725	0.9	0.0	500	0.72
39	10	295	470	0.6	-0.3	500	0.76
40	10	3850	4065	0.0	-0.3	400	0.81
41	10	4720	4845	0.3	-0.3	400	0.82
42	11	3715	4120	0.0	-0.6	400	0.71
43	12	1555	1720	0.0	0.0	400	0.74
44	12	4470	4655	0.6	-0.6	500	0.73
45	12	5115	5290	0.0	-0.6	400	0.78
46	12	805	1075	0.0	0.0	400	0.66
47	13	1195	1305	0.0	-0.3	500	0.76
48	13	1980	2305	0.0	-0.3	400	0.68
49	13	5175	5560	0.0	0.0	400	0.66
50	14	3090	3240	0.3	0.0	500	0.75
51	14	4445	4595	0.0	0.0	400	0.76
52	15	4990	5126	0.0	-0.6	400	0.78
53	16	3865	4120	0.0	-0.6	400	0.73
54	18	770	1190	0.9	-0.6	500	0.72
55	20	1570	1670	0.0	-0.3	400	0.81
56	21	1405	1625	0.0	-0.6	400	0.71
57	21	1745	1920	0.6	-0.3	500	0.77
58	21	2030	2240	0.6	-0.6	400	0.78
59	23	6470	6575	0.0	0.0	500	0.71
60	23	6860	6990	0.9	0.0	600	0.62
61	23	790	935	0.6	-0.3	500	0.76

CC corresponds to the correlation coefficient of a contact map based on the 3D models and the input HiC data for the region. High correlation coefficients are indicative of the bona fide representation of the HiC data by the models.

Supplementary Table 3: Summary of modelled TADs coordinates

	Region	TAD id	Chr	Coords Ini	Coords End	Bin Ini	Bin End	Par Ini	Par End	Par Len	Length	Type
1	1	27	1	36,300,000	36,900,000	1,815	1,845	1	31	30	600,000	NA
2		28	1	36,900,000	38,000,000	1,845	1,900	31	86	55	1,100,000	UP
3		29	1	38,000,000	38,500,000	1,900	1,925	86	111	25	500,000	NA
4	2	40	1	60,300,000	62,400,000	3,015	3,120	1	106	105	2,100,000	NA
5		41	1	62,400,000	63,300,000	3,120	3,165	106	151	45	900,000	DOWN
6		42	1	63,300,000	64,000,000	3,165	3,200	151	186	35	700,000	NA
7	3	84	1	116,600,000	117,100,000	5,830	5,855	1	26	25	500,000	NA
8		85	1	117,100,000	118,500,000	5,855	5,925	26	96	70	1,400,000	DOWN
9		86	1	118,500,000	120,000,000	5,925	6,000	96	171	75	1,500,000	NA
10	4	105	1	167,500,000	168,200,000	8,375	8,410	1	36	35	700,000	NA
11		106	1	168,200,000	169,500,000	8,410	8,475	36	101	65	1,300,000	UP
12		107	1	169,500,000	171,500,000	8,475	8,575	101	201	100	2,000,000	NA
13	5	121	1	181,400,000	182,000,000	9,070	9,100	1	31	30	600,000	NA
14		122	1	182,000,000	182,900,000	9,100	9,145	31	76	45	900,000	UP
15		123	1	182,900,000	186,300,000	9,145	9,315	76	246	170	3,400,000	NA
16	6	130	1	210,000,000	210,500,000	10,500	10,525	1	26	25	500,000	NA
17		131	1	210,500,000	211,500,000	10,525	10,575	26	76	50	1,000,000	UP
18		132	1	211,500,000	213,200,000	10,575	10,660	76	161	85	1,700,000	NA
19	7	144	1	226,300,000	228,800,000	11,315	11,440	1	126	125	2,500,000	NA
20		145	1	228,800,000	229,700,000	11,440	11,485	126	171	45	900,000	UP
21		146	1	229,700,000	230,600,000	11,485	11,530	171	216	45	900,000	UP
22		147	1	230,600,000	231,800,000	11,530	11,590	216	276	60	1,200,000	NA
23	8	169	2	9,600,000	10,800,000	480	540	1	61	60	1,200,000	NA
24		170	2	10,800,000	11,900,000	540	595	61	116	55	1,100,000	UP
25		171	2	11,900,000	13,200,000	595	660	116	181	65	1,300,000	NA
26	9	190	2	42,100,000	43,000,000	2,105	2,150	1	46	45	900,000	NA
27		191	2	43,000,000	43,900,000	2,150	2,195	46	91	45	900,000	DOWN
28		192	2	43,900,000	45,800,000	2,195	2,290	91	186	95	1,900,000	NA
29	10	206	2	69,600,000	70,500,000	3,480	3,525	1	46	45	900,000	NA
30		207	2	70,500,000	71,300,000	3,525	3,565	46	86	40	800,000	UP
31		208	2	71,300,000	73,400,000	3,565	3,670	86	191	105	2,100,000	NA
32		209	2	73,400,000	73,900,000	3,670	3,695	191	216	25	500,000	NA
33		210	2	73,900,000	74,900,000	3,695	3,745	216	266	50	1,000,000	NA
34		211	2	74,900,000	75,900,000	3,745	3,795	266	316	50	1,000,000	UP
35		212	2	75,900,000	80,200,000	3,795	4,010	316	531	215	4,300,000	NA
36	11	260	2	158,200,000	158,800,000	7,910	7,940	1	31	30	600,000	NA
37		261	2	158,800,000	159,700,000	7,940	7,985	31	76	45	900,000	DOWN
38		262	2	159,700,000	160,900,000	7,985	8,045	76	136	60	1,200,000	NA
39	12	291	2	198,800,000	200,800,000	9,940	10,040	1	101	100	2,000,000	NA
40		292	2	200,800,000	201,700,000	10,040	10,085	101	146	45	900,000	UP
41		293	2	201,700,000	202,600,000	10,085	10,130	146	191	45	900,000	NA
42	13	306	2	220,500,000	222,900,000	11,025	11,145	1	121	120	2,400,000	NA
43		307	2	222,900,000	223,800,000	11,145	11,190	121	166	45	900,000	UP
44		308	2	223,800,000	224,800,000	11,190	11,240	166	216	50	1,000,000	NA
45	14	422	3	150,300,000	152,700,000	7,515	7,635	1	121	120	2,400,000	NA
46		423	3	152,700,000	154,000,000	7,635	7,700	121	186	65	1,300,000	UP
47		424	3	154,000,000	155,200,000	7,700	7,760	186	246	60	1,200,000	NA
48		425	3	155,200,000	155,700,000	7,760	7,785	246	271	25	500,000	NA
49		426	3	155,700,000	156,900,000	7,785	7,845	271	331	60	1,200,000	UP
50		427	3	156,900,000	158,400,000	7,845	7,920	331	406	75	1,500,000	NA
51	15	435	3	167,900,000	168,600,000	8,395	8,430	1	36	35	700,000	NA
52		436	3	168,600,000	169,500,000	8,430	8,475	36	81	45	900,000	DOWN
53		437	3	169,500,000	170,000,000	8,475	8,500	81	106	25	500,000	NA
54	16	470	4	7,100,000	8,200,000	355	410	1	56	55	1,100,000	NA
55		471	4	8,200,000	9,000,000	410	450	56	96	40	800,000	DOWN
56		472	4	9,000,000	9,800,000	450	490	96	136	40	800,000	NA
57	17	494	4	39,400,000	40,000,000	1,970	2,000	1	31	30	600,000	NA
58		495	4	40,000,000	40,800,000	2,000	2,040	31	71	40	800,000	DOWN
59		496	4	40,800,000	42,000,000	2,040	2,100	71	131	60	1,200,000	NA
60	18	517	4	79,800,000	81,200,000	3,990	4,060	1	71	70	1,400,000	NA
61		518	4	81,200,000	82,100,000	4,060	4,105	71	116	45	900,000	DOWN
62		519	4	82,100,000	83,300,000	4,105	4,165	116	176	60	1,200,000	NA
63	19	526	4	88,200,000	90,000,000	4,410	4,500	1	91	90	1,800,000	NA
64		527	4	90,000,000	91,200,000	4,500	4,560	91	151	60	1,200,000	DOWN
65		528	4	91,200,000	95,200,000	4,560	4,760	151	351	200	4,000,000	NA
66	20	535	4	104,900,000	106,400,000	5,245	5,320	1	76	75	1,500,000	NA
67		536	4	106,400,000	107,200,000	5,320	5,360	76	116	40	800,000	DOWN
68		537	4	107,200,000	108,700,000	5,360	5,435	116	191	75	1,500,000	UP
69		538	4	108,700,000	109,600,000	5,435	5,480	191	236	45	900,000	NA
70	21	600	5	10,700,000	14,000,000	535	700	1	166	165	3,300,000	NA
71		601	5	14,000,000	15,000,000	700	750	166	216	50	1,000,000	UP
72		602	5	15,000,000	16,200,000	750	810	216	276	60	1,200,000	NA
73	22	631	5	52,100,000	54,500,000	2,605	2,725	1	121	120	2,400,000	NA
74		632	5	54,500,000	55,500,000	2,725	2,775	121	171	50	1,000,000	UP
75		633	5	55,500,000	56,200,000	2,775	2,810	171	206	35	700,000	NA
76		634	5	56,200,000	56,700,000	2,810	2,835	206	231	25	500,000	NA
77		635	5	56,700,000	57,800,000	2,835	2,890	231	286	55	1,100,000	DOWN
78		636	5	57,800,000	58,300,000	2,890	2,915	286	311	25	500,000	NA
79	23	691	5	141,000,000	142,100,000	7,050	7,105	1	56	55	1,100,000	NA
80		692	5	142,100,000	143,600,000	7,105	7,180	56	131	75	1,500,000	UP
81		693	5	143,600,000	145,200,000	7,180	7,260	131	211	80	1,600,000	NA
82		694	5	145,200,000	145,900,000	7,260	7,295	211	246	35	700,000	NA
83		695	5	145,900,000	147,000,000	7,295	7,350	246	301	55	1,100,000	UP
84		696	5	147,000,000	148,100,000	7,350	7,405	301	356	55	1,100,000	NA
85	24	758	6	53,600,000	56,200,000	2,680	2,810	1	131	130	2,600,000	NA
86		759	6	56,200,000	57,200,000	2,810	2,860	131	181	50	1,000,000	DOWN
87		760	6	57,200,000	64,000,000	2,860	3,200	181	521	340	6,800,000	NA
88	25	766	6	71,800,000	72,800,000	3,590	3,640	1	51	50	1,000,000	NA
89		767	6	72,800,000	74,200,000	3,640	3,710	51	121	70	1,400,000	DOWN
90		768	6	74,200,000	76,500,000	3,710	3,825	121	236	115	2,300,000	NA
91	26	820	6	151,200,000	151,700,000	7,560	7,585	1	26	25	500,000	NA
92		821	6	151,700,000	152,700,000	7,585	7,635	26	76	50	1,000,000	DOWN
93		822	6	152,700,000	153,300,000	7,635	7,665	76	106	30	600,000	NA
94	27	827	6	157,700,000	158,600,000	7,885	7,930	1	46	45	900,000	NA
95		828	6	158,600,000	159,400,000	7,930	7,970	46	86	40	800,000	UP
96		829	6	159,400,000	161,100,000	7,970	8,055	86	171	85	1,700,000	NA
97	28	868	7	48,200,000	50,100,000	2,410	2,505	1	96	95	1,900,000	NA
98		869	7	50,100,000	51,400,000	2,505	2,570	96	161	65	1,300,000	UP
99		870	7	51,400,000	54,800,000	2,570	2,740	161	331	170	3,400,000	NA
100	29	883	7	87,800,000	90,100,000	4,390	4,505	1	116	115	2,300,000	NA
101		884	7	90,100,000	91,600,000	4,505	4,580	116	191	75	1,500,000	UP
102		885	7	91,600,000	92,200,000	4,580	4,610	191	221	30	600,000	NA
103	30	927	7	156,600,000	157,200,000	7,830	7,860	1	31	30	600,000	NA
104		928	7	157,200,000	158,200,000	7,860	7,910	31	81	50	1,000,000	UP
105		929	7	158,200,000	159,200,000	7,910	7,960	81	131	50	1,000,000	NA
106	31	938	8	9,100,000	9,700,000	455	485	1	31	30	600,000	NA

	Region	TAD id	Chr	Coords Ini	Coords End	Bin Ini	Bin End	Par Ini	Par End	Par Len	Length	Type
107		939	8	9,700,000	11,200,000	485	560	31	106	75	1,500,000	UP
108		940	8	11,200,000	11,900,000	560	595	106	141	35	700,000	NA
109	32	974	8	53,500,000	55,400,000	2,675	2,770	1	96	95	1,900,000	NA
110		975	8	55,400,000	56,500,000	2,770	2,825	96	151	55	1,100,000	UP
111		976	8	56,500,000	57,000,000	2,825	2,850	151	176	25	500,000	NA
112	33	1012	8	103,900,000	104,700,000	5,195	5,235	1	41	40	800,000	NA
113		1013	8	104,700,000	105,500,000	5,235	5,275	41	81	40	800,000	DOWN
114		1014	8	105,500,000	106,900,000	5,275	5,345	81	151	70	1,400,000	NA
115	34	1044	9	0	1,000,000	0	50	1	51	50	1,000,000	UP
116		1045	9	1,000,000	2,100,000	50	105	51	106	55	1,100,000	NA
117	35	1100	9	117,100,000	123,400,000	5,855	6,170	1	316	315	6,300,000	NA
118		1101	9	123,400,000	124,200,000	6,170	6,210	316	356	40	800,000	UP
119		1102	9	124,200,000	124,800,000	6,210	6,240	356	386	30	600,000	NA
120	36	1118	9	139,200,000	140,400,000	6,960	7,020	1	61	60	1,200,000	NA
121		1119	9	140,400,000	141,300,000	7,020	7,065	61	106	45	900,000	UP
122	37	1126	10	5,900,000	6,500,000	295	325	1	31	30	600,000	NA
123		1127	10	6,500,000	7,700,000	325	385	31	91	60	1,200,000	DOWN
124		1128	10	7,700,000	9,400,000	385	470	91	176	85	1,700,000	NA
125	38	1135	10	21,300,000	23,400,000	1,065	1,170	1	106	105	2,100,000	NA
126		1136	10	23,400,000	24,900,000	1,170	1,245	106	181	75	1,500,000	DOWN
127		1137	10	24,900,000	26,000,000	1,245	1,300	181	236	55	1,100,000	NA
128		1138	10	26,000,000	26,900,000	1,300	1,345	236	281	45	900,000	NA
129		1139	10	26,900,000	27,600,000	1,345	1,380	281	316	35	700,000	NA
130		1140	10	27,600,000	28,700,000	1,380	1,435	316	371	55	1,100,000	DOWN
131		1141	10	28,700,000	29,700,000	1,435	1,485	371	421	50	1,000,000	DOWN
132		1142	10	29,700,000	30,900,000	1,485	1,545	421	481	60	1,200,000	NA
133	39	1157	10	51,900,000	52,500,000	2,595	2,625	1	31	30	600,000	NA
134		1158	10	52,500,000	54,000,000	2,625	2,700	31	106	75	1,500,000	DOWN
135		1159	10	54,000,000	54,500,000	2,700	2,725	106	131	25	500,000	NA
136	40	1172	10	77,000,000	78,900,000	3,850	3,945	1	96	95	1,900,000	NA
137		1173	10	78,900,000	79,800,000	3,945	3,990	96	141	45	900,000	UP
138		1174	10	79,800,000	81,300,000	3,990	4,065	141	216	75	1,500,000	NA
139	41	1185	10	94,400,000	95,500,000	4,720	4,775	1	56	55	1,100,000	NA
140		1186	10	95,500,000	96,300,000	4,775	4,815	56	96	40	800,000	UP
141		1187	10	96,300,000	96,900,000	4,815	4,845	96	126	30	600,000	NA
142	42	1273	11	74,300,000	77,400,000	3,715	3,870	1	156	155	3,100,000	NA
143		1274	11	77,400,000	78,300,000	3,870	3,915	156	201	45	900,000	DOWN
144		1275	11	78,300,000	82,400,000	3,915	4,120	201	406	205	4,100,000	NA
145	43	1331	12	16,100,000	18,300,000	805	915	1	111	110	2,200,000	NA
146		1332	12	18,300,000	19,700,000	915	985	111	181	70	1,400,000	DOWN
147		1333	12	19,700,000	21,500,000	985	1,075	181	271	90	1,800,000	NA
148	44	1340	12	31,100,000	31,600,000	1,555	1,580	1	26	25	500,000	NA
149		1341	12	31,600,000	32,900,000	1,580	1,645	26	91	65	1,300,000	UP
150		1342	12	32,900,000	34,400,000	1,645	1,720	91	166	75	1,500,000	NA
151	45	1381	12	89,400,000	89,900,000	4,470	4,495	1	26	25	500,000	NA
152		1382	12	89,900,000	91,400,000	4,495	4,570	26	101	75	1,500,000	DOWN
153		1383	12	91,400,000	93,100,000	4,570	4,655	101	186	85	1,700,000	NA
154	46	1389	12	102,300,000	103,200,000	5,115	5,160	1	46	45	900,000	NA
155		1390	12	103,200,000	104,000,000	5,160	5,200	46	86	40	800,000	DOWN
156		1391	12	104,000,000	105,800,000	5,200	5,290	86	176	90	1,800,000	NA
157	47	1420	13	23,900,000	24,700,000	1,195	1,235	1	41	40	800,000	NA
158		1421	13	24,700,000	25,600,000	1,235	1,280	41	86	45	900,000	UP
159		1422	13	25,600,000	26,100,000	1,280	1,305	86	111	25	500,000	NA
160	48	1435	13	39,600,000	40,300,000	1,980	2,015	1	36	35	700,000	NA
161		1436	13	40,300,000	41,400,000	2,015	2,070	36	91	55	1,100,000	UP
162		1437	13	41,400,000	41,900,000	2,070	2,095	91	116	25	500,000	NA
163		1438	13	41,900,000	42,900,000	2,095	2,145	116	166	50	1,000,000	NA
164		1439	13	42,900,000	44,500,000	2,145	2,225	166	246	80	1,600,000	NA
165		1440	13	44,500,000	45,600,000	2,225	2,280	246	301	55	1,100,000	UP
166		1441	13	45,600,000	46,100,000	2,280	2,305	301	326	25	500,000	NA
167	49	1477	13	103,500,000	107,800,000	5,175	5,390	1	216	215	4,300,000	NA
168		1478	13	107,800,000	108,900,000	5,390	5,445	216	271	55	1,100,000	DOWN
169		1479	13	108,900,000	111,200,000	5,445	5,560	271	386	115	2,300,000	NA
170	50	1506	14	61,800,000	62,300,000	3,090	3,115	1	26	25	500,000	NA
171		1507	14	62,300,000	63,800,000	3,115	3,190	26	101	75	1,500,000	DOWN
172		1508	14	63,800,000	64,800,000	3,190	3,240	101	151	50	1,000,000	NA
173	51	1523	14	88,900,000	89,400,000	4,445	4,470	1	26	25	500,000	NA
174		1524	14	89,400,000	90,400,000	4,470	4,520	26	76	50	1,000,000	UP
175		1525	14	90,400,000	91,900,000	4,520	4,595	76	151	75	1,500,000	NA
176	52	1608	15	99,800,000	100,300,000	4,990	5,015	1	26	25	500,000	NA
177		1609	15	100,300,000	101,100,000	5,015	5,055	26	66	40	800,000	UP
178		1610	15	101,100,000	102,600,000	5,055	5,130	66	141	75	1,500,000	NA
179	53	1666	16	77,300,000	81,000,000	3,865	4,050	1	186	185	3,700,000	NA
180		1667	16	81,000,000	81,900,000	4,050	4,095	186	231	45	900,000	UP
181		1668	16	81,900,000	82,400,000	4,095	4,120	231	256	25	500,000	NA
182	54	1750	18	15,400,000	19,400,000	770	970	1	201	200	4,000,000	NA
183		1751	18	19,400,000	20,300,000	970	1,015	201	246	45	900,000	UP
184		1752	18	20,300,000	21,100,000	1,015	1,055	246	286	40	800,000	NA
185		1753	18	21,100,000	22,000,000	1,055	1,100	286	331	45	900,000	UP
186		1754	18	22,000,000	23,800,000	1,100	1,190	331	421	90	1,800,000	NA
187	55	1860	20	31,400,000	31,900,000	1,570	1,595	1	26	25	500,000	NA
188		1861	20	31,900,000	32,800,000	1,595	1,640	26	71	45	900,000	UP
189		1862	20	32,800,000	33,400,000	1,640	1,670	71	101	30	600,000	NA
190	56	1900	21	28,100,000	30,400,000	1,405	1,520	1	116	115	2,300,000	NA
191		1901	21	30,400,000	31,700,000	1,520	1,585	116	181	65	1,300,000	DOWN
192		1902	21	31,700,000	32,500,000	1,585	1,625	181	221	40	800,000	NA
193	57	1906	21	34,900,000	36,000,000	1,745	1,800	1	56	55	1,100,000	NA
194		1907	21	36,000,000	37,500,000	1,800	1,875	56	131	75	1,500,000	UP
195		1908	21	37,500,000	38,400,000	1,875	1,920	131	176	45	900,000	NA
196	58	1912	21	40,600,000	41,100,000	2,030	2,055	1	26	25	500,000	NA
197		1913	21	41,100,000	42,600,000	2,055	2,130	26	101	75	1,500,000	DOWN
198		1914	21	42,600,000	43,300,000	2,130	2,165	101	136	35	700,000	NA
199		1915	21	43,300,000	44,100,000	2,165	2,205	136	176	40	800,000	DOWN
200		1916	21	44,100,000	44,800,000	2,205	2,240	176	211	35	700,000	NA
201	59	1967	X	15,800,000	16,800,000	790	840	1	51	50	1,000,000	NA
202		1968	X	16,800,000	18,000,000	840	900	51	111	60	1,200,000	UP
203		1969	X	18,000,000	18,700,000	900	935	111	146	35	700,000	NA
204	60	2013	X	129,400,000	130,100,000	6,470	6,505	1	36	35	700,000	NA
205		2014	X	130,100,000	130,900,000	6,505	6,545	36	76	40	800,000	DOWN
206		2015	X	130,900,000	131,500,000	6,545	6,575	76	106	30	600,000	NA
207	61	2019	X	137,200,000	137,800,000	6,860	6,890	1	31	30	600,000	NA
208		2020	X	137,800,000	139,100,000	6,890	6,955	31	96	65	1,300,000	UP
209		2021	X	139,100,000	139,800,000	6,955	6,990	96	131	35	700,000	NA

3. Supplementary References

Ballare C, Castellano G, Gaveglia L, Althammer S, Gonzalez-Vallinas J, Eyras E, Le Dily F, Zaurin R, Soronellas D, Vicent GP et al. 2013. Nucleosome-driven transcription factor binding and gene regulation. *Molecular cell* **49**(1): 67-79.

Bau D, Marti-Renom MA. 2012. Genome structure determination via 3C-based data integration by the Integrative Modeling Platform. *Methods* **58**(3): 300-306.

Enright AJ, Van Dongen S, Ouzounis CA. 2002. An efficient algorithm for large-scale detection of protein families. *Nucleic acids research* **30**(7): 1575-1584.

Harp JM, Hanson BL, Timm DE, Bunick GJ. 2000. Asymmetries in the nucleosome core particle at 2.5 A resolution. *Acta crystallographica Section D, Biological crystallography* **56**(Pt 12): 1513-1534.

Harrow J, Frankish A, Gonzalez JM, Tapanari E, Diekhans M, Kokocinski F, Aken BL, Barrell D, Zadissa A, Searle S et al. 2012. GENCODE: the reference human genome annotation for The ENCODE Project. *Genome research* **22**(9): 1760-1774.

Lieberman-Aiden E, van Berkum NL, Williams L, Imakaev M, Ragoczy T, Telling A, Amit I, Lajoie BR, Sabo PJ, Dorschner MO et al. 2009. Comprehensive mapping of long-range interactions reveals folding principles of the human genome. *Science* **326**(5950): 289-293.

Marco-Sola S, Sammeth M, Guigo R, Ribeca P. 2012. The GEM mapper: fast, accurate and versatile alignment by filtration. *Nature methods* **9**(12): 1185-1188.

Montgomery SB, Sammeth M, Gutierrez-Arcelus M, Lach RP, Ingle C, Nisbett J, Guigo R, Dermitzakis ET. 2010. Transcriptome genetics using second generation sequencing in a Caucasian population. *Nature* **464**(7289): 773-777.

Pique-Regi R, Monso-Varona J, Ortega A, Seeger RC, Triche TJ, Asgharzadeh S. 2008. Sparse representation and Bayesian detection of genome copy number alterations from microarray data. *Bioinformatics* **24**(3): 309-318.

Vicent GP, Nacht AS, Zaurin R, Font-Mateu J, Soronellas D, Le Dily F, Reyes D, Beato M. 2013. Unliganded progesterone receptor-mediated targeting of an RNA-containing repressive complex silences a subset of hormone-inducible genes. *Genes Dev* **27**(10): 1179-1197.

Wang L, Wang S, Li W. 2012. RSeQC: quality control of RNA-seq experiments. *Bioinformatics* **28**(16): 2184-2185.

Yang Z, Lasker K, Schneidman-Duhovny D, Webb B, Huang CC, Pettersen EF, Goddard TD, Meng EC, Sali A, Ferrin TE. 2012. UCSF Chimera, MODELLER, and IMP: an integrated modeling system. *Journal of structural biology* **179**(3): 269-278.

4. Supplementary Figures and legends

Supplementary Figure 1: T47D genome is organised in TADs.

(A) The linear correlation between number of Hi-C contacts and number of restriction sites is lost due to changes in copy number allowing determining the number of copies of each megabase domains present in T47D genome (top left panel). A snapshot of contact matrix shows an example of translocation breackpoint between the chromosomes 7 and 15 in T47D cells (top middle panel). T47D karyotype deduced from the variations in copy number and translocations events determined as above is represented (right panel). Bottom left panel show examples of 2D-FISH on T47D cells metaphase spreads validating the karyotype and highlighting changes in ploidy, translocation events as well as normal chromosomes. **(B)** Distribution of boundaries confidence scores for TADs defined at 40 (light grey – n=3027) or 100 Kb (dark grey – n=2031) resolutions. **(C)** Distribution of TAD sizes determined at 100 Kb resolution (N genome=2031).

Supplementary Figure 2: Functional characterization of TADs.

TADs were divided into 5 sub-segments of equal size to study the distribution of epigenetic features according a border (b) to center (c) distribution (see Supplementary Methods). **(A)** The median percentage of Transcription Start Sites of protein coding genes (TSS), RNA-Polymerase II (Pol.II), and CTCF binding sites, as well as DNAse I hypersensitive sites (DHS) is shown. **(B)** The histogram represent the median ratio of normalised ChIP-Seq signals over input for H3K36me3, H3K27me3, H3K9me3 and total H4 determined in the TADs 5 sub-segments. **(C)** Normalised ChIP-Seq signals over input ratio were calculated per sub-segment for each TAD for the indicated chromatin components and marks mentioned. Histograms show, for each mark, the median normalised signal/Input observed in the 5 sub-segments for all TADs in the genome.

Supplementary Figure 3: TADs are epigenetic domains which chromatin is coordinately modified upon Pg.

(A) Plots show the homogeneity score of the normalised Chip-Seq signal/Input ratio between successive sub-segments (see Supplementary Methods) over 3

consecutive TADs for the chromatin marks and components listed. Lines depict the 25th, 50th and 75th percentiles (from top to bottom respectively) of the scores computed genome-wide. **(B)** Differences of +Pg/-Pg H3K9me3 Chip-Seq signal between consecutive sub-segments (see Fig. S3 and Supplementary information) over 3 consecutive TADs in the case of observed (*left panel*) or randomized (*right panel*) TADs borders show that transition between Pg induced changes in chromatin state occur preferentially at the TAD boundaries. Similar analysis was performed for other chromatin marks as example H3K27me3 and H3K36me2.

Supplementary Figure 4: Homogeneous and specific response of TADs to steroid hormones.

(A) The ratio of normalised reads after and before 6 hour of treatment with Pg were calculated for each TAD. The scatter plot shows the correlation of response to Pg per TAD obtained in two biological replicates (BR1 and BR2) of RNA-Seq. **(B)** Boxplots show the basal expression levels (RPKM – Log_2) of genes located within the three types of TADs. **(C)** Scatter plot showing the correlation of response per TAD after 6 hours of treatment with Pg (R6) with the changes obtained after 1 hour of Pg induction (R1) or 6 hours of treatment with E2 (E6).

Supplementary Figure 5: TADs respond as unit to the hormone stimulus

(A and B) Genome browser view of RNA-Seq signal within TADs presented in Figure 2E (**(A)** U469; **(B)** U821) highlighting the expression of non-annotated non-coding transcripts which correlate with the hormone induced changes in expression observed for the protein coding genes.

Supplementary Figure 6: Structural changes of TADs.

(A and B) Distributions of the changes of intra-TAD contacts proportions upon Pg treatment (See Extended Experimental Procedures) in the different TAD categories for the two independent datasets obtained with *HindIII* (**A**) or *NcoI* (**B**). Boxplot whiskers correspond to 5st and 95th percentiles. (***),(**),(*) indicate P < 0.0001, 0.001 and 0.01, respectively (Mann-Whitney test). **(C)** Pair-wise inter-probes 3D distances obtained in the models (left panel) or *in situ* (right panel) were plotted

according the genomic distances that separate them. **(D)** Distributions of the accessibility scores calculated from the models for particles containing or not a TSS.

A

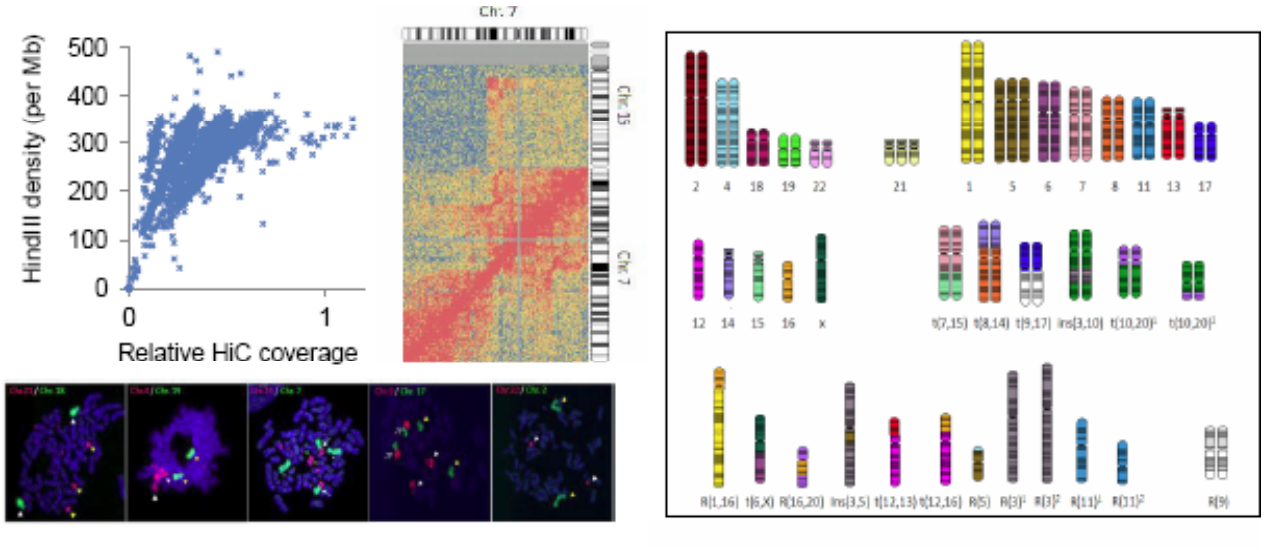
HindIII density (per Mb)
500
400
300
200
100
0
0
1
Relative HiC coverage
Chr. 7
Chr 15
Chr 7

B

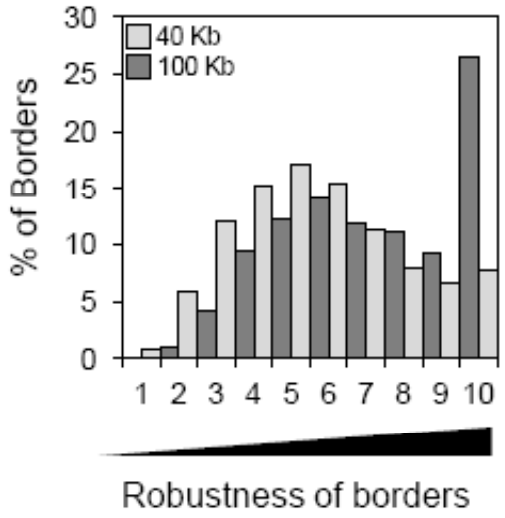
% of Borders
30
25
20
15
10
5
0
40 Kb
100 Kb
1 2 3 4 5 6 7 8 9 10
Robustness of borders

C

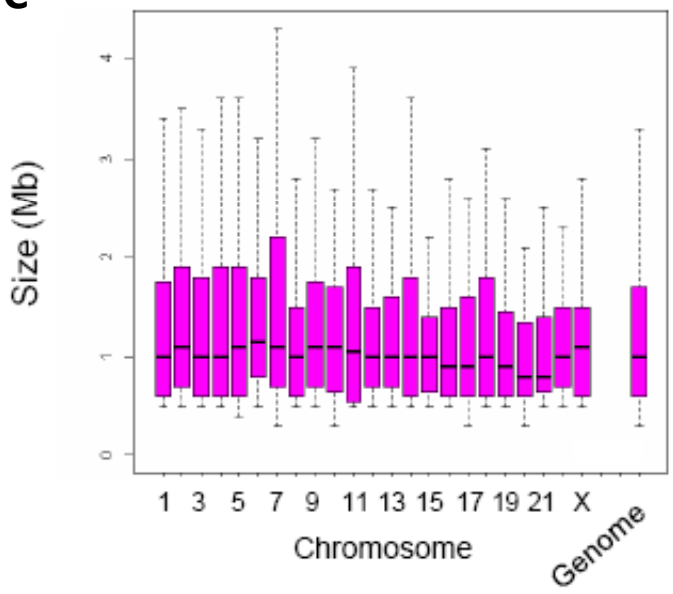
Size (Mb)
0
1
2
3
4
1 3 5 7 9 11 13 15 17 19 21 X
Chromosome
Genome

Le Dily_Fig. S2

A

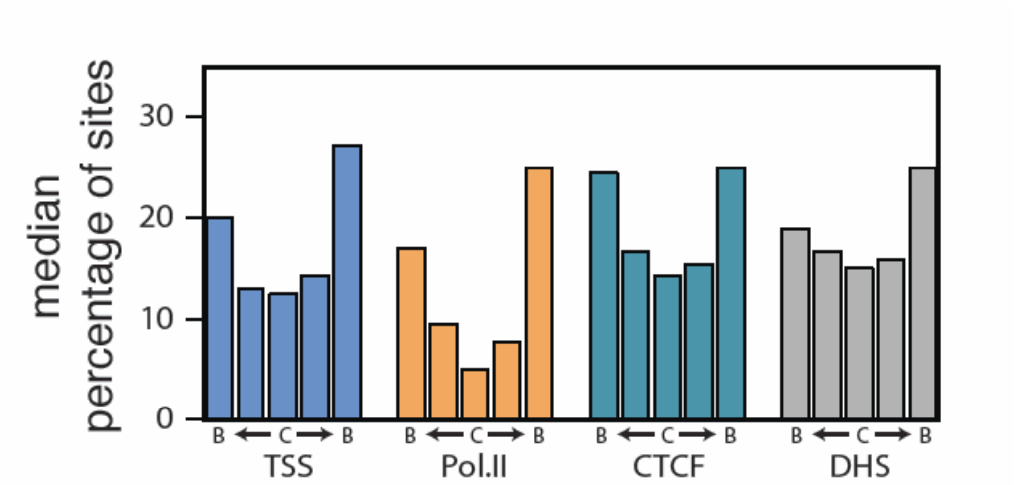

B

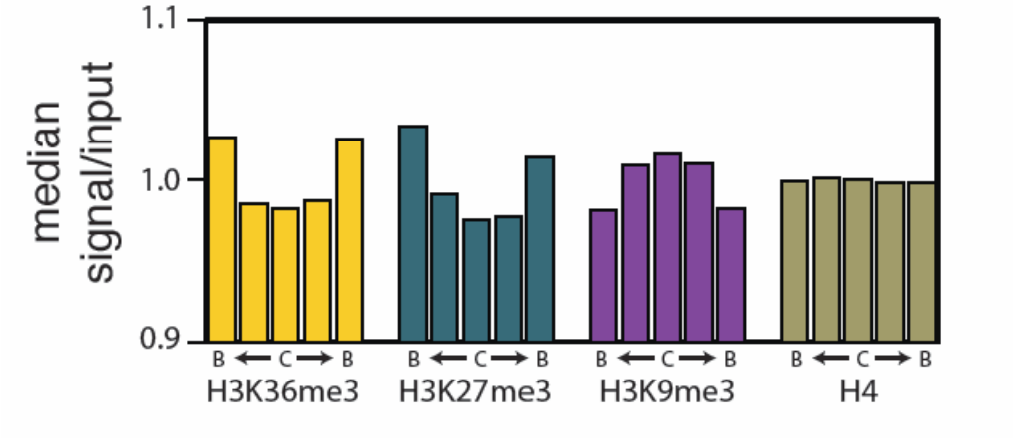

C

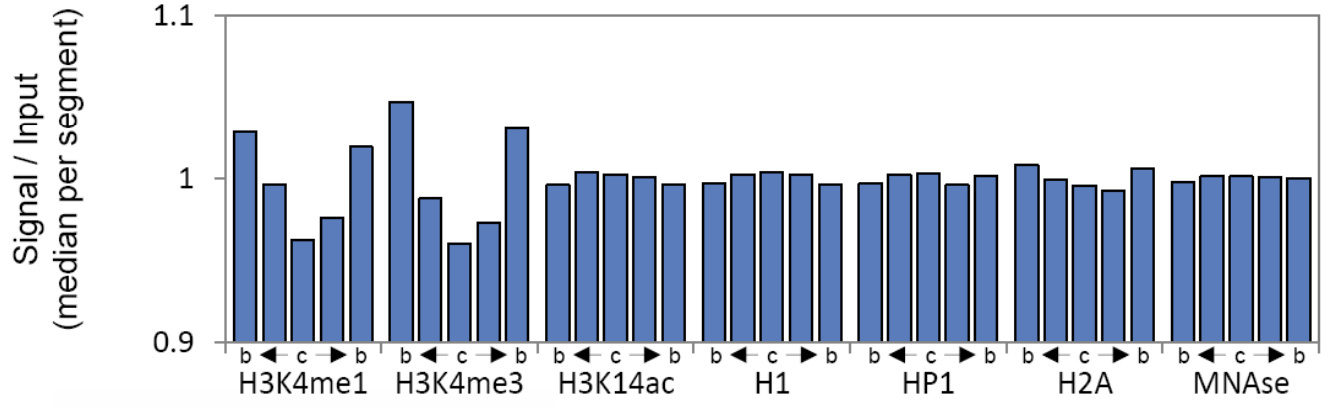

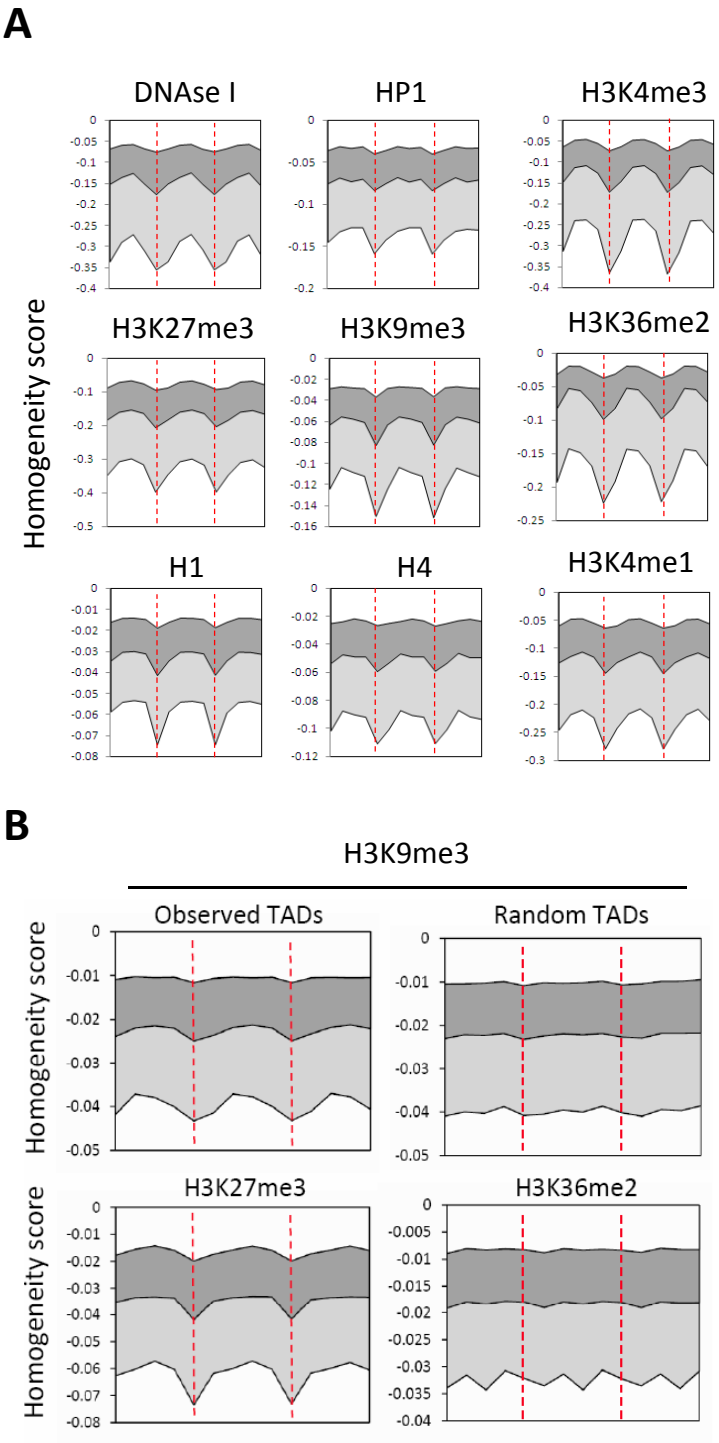
A
DNAse I
HP1
H3K4me3
H3K27me3
H3K9me3
H3K36me2
H1
H4
H3K4me1
Homogeneity score
B
H3K9me3
Observed TADs
Random TADs
H3K27me3
H3K36me2
Homogeneity score
Homogeneity score

Le Dily_Fig. S4

A

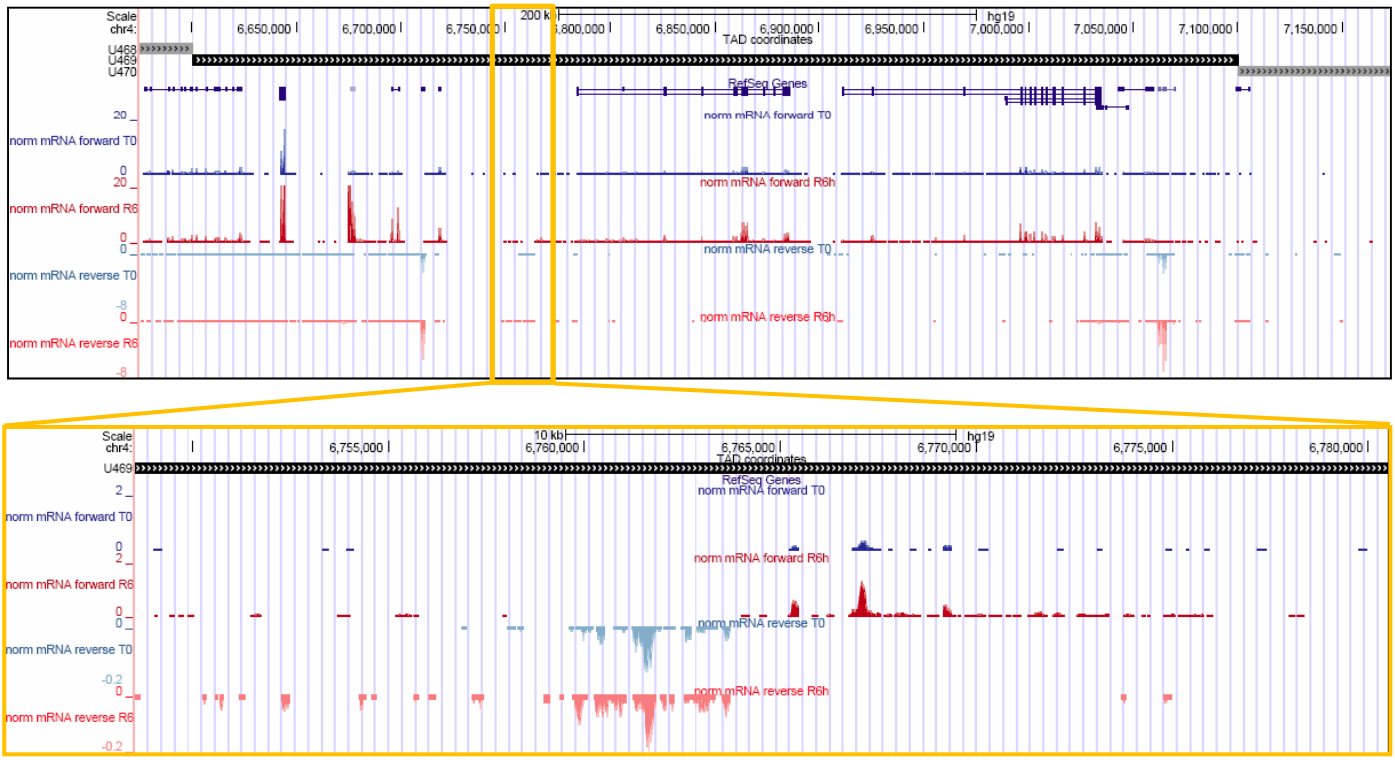

B

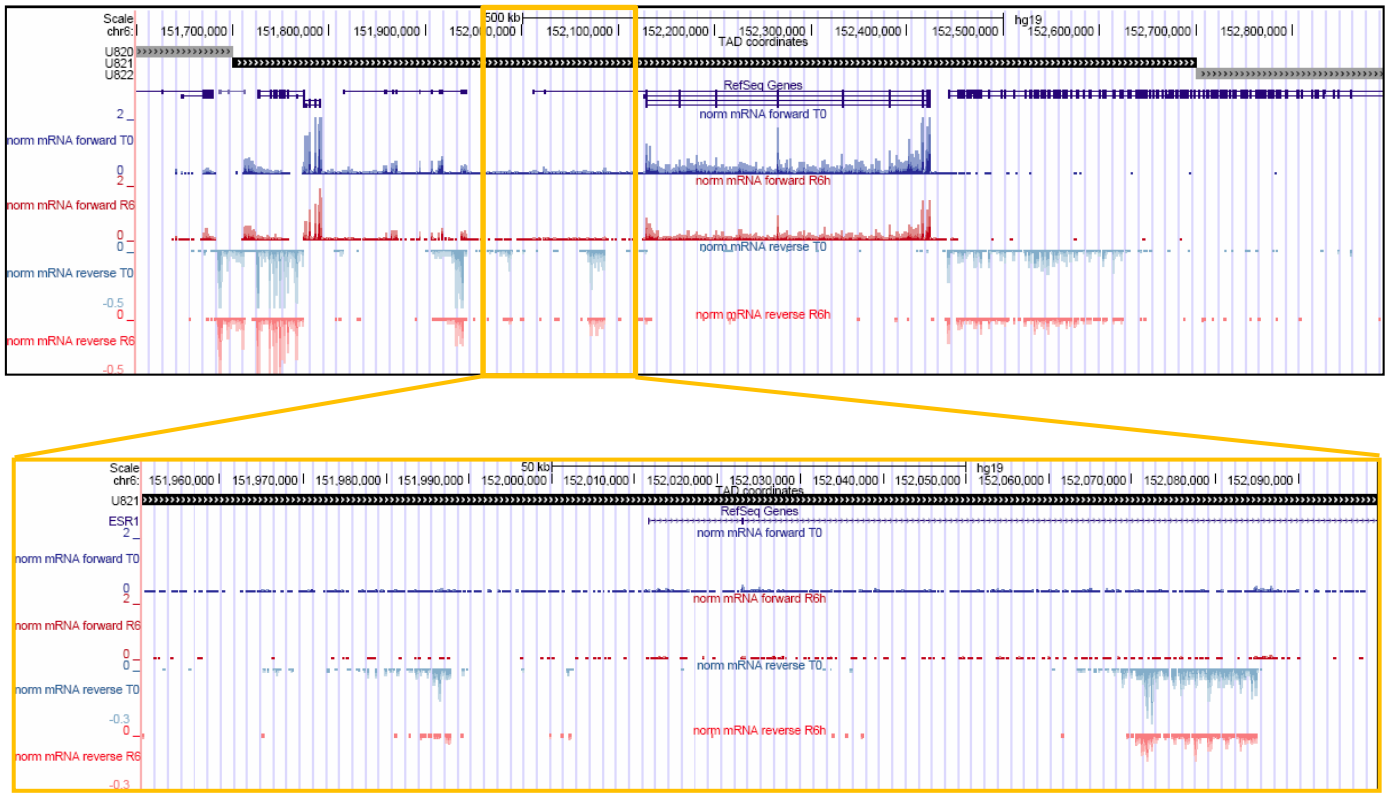

Le Dily_Fig. S5

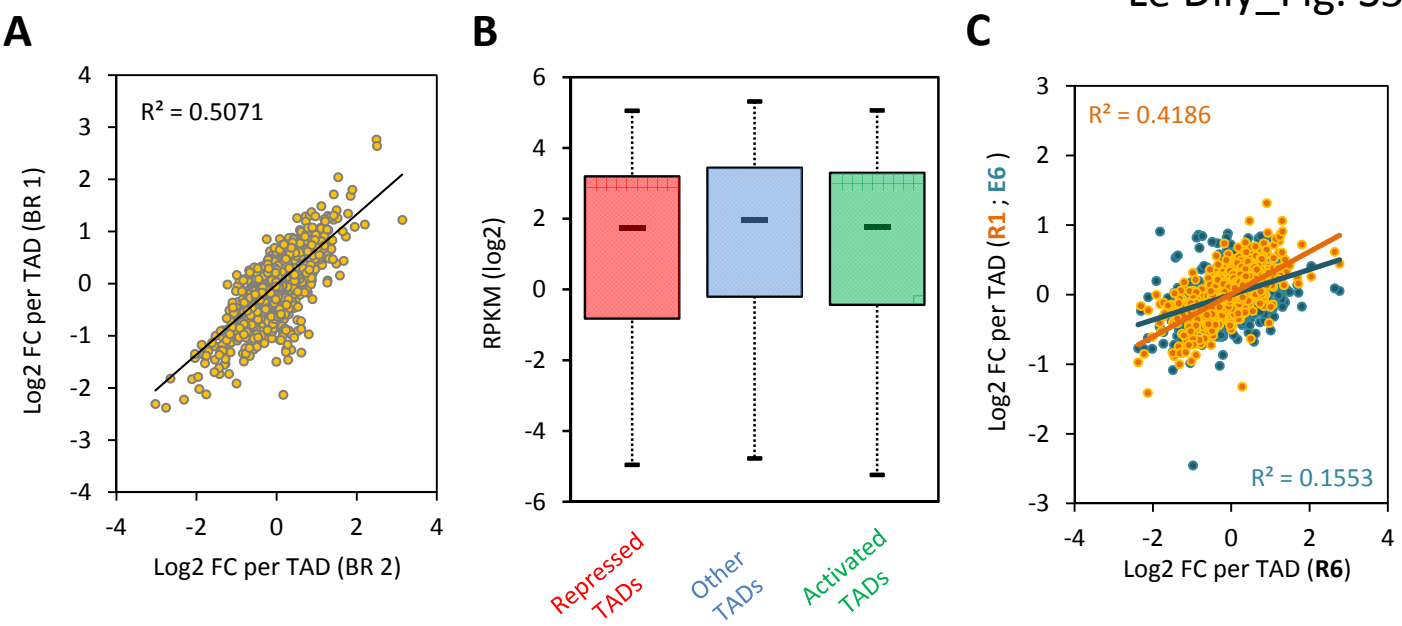

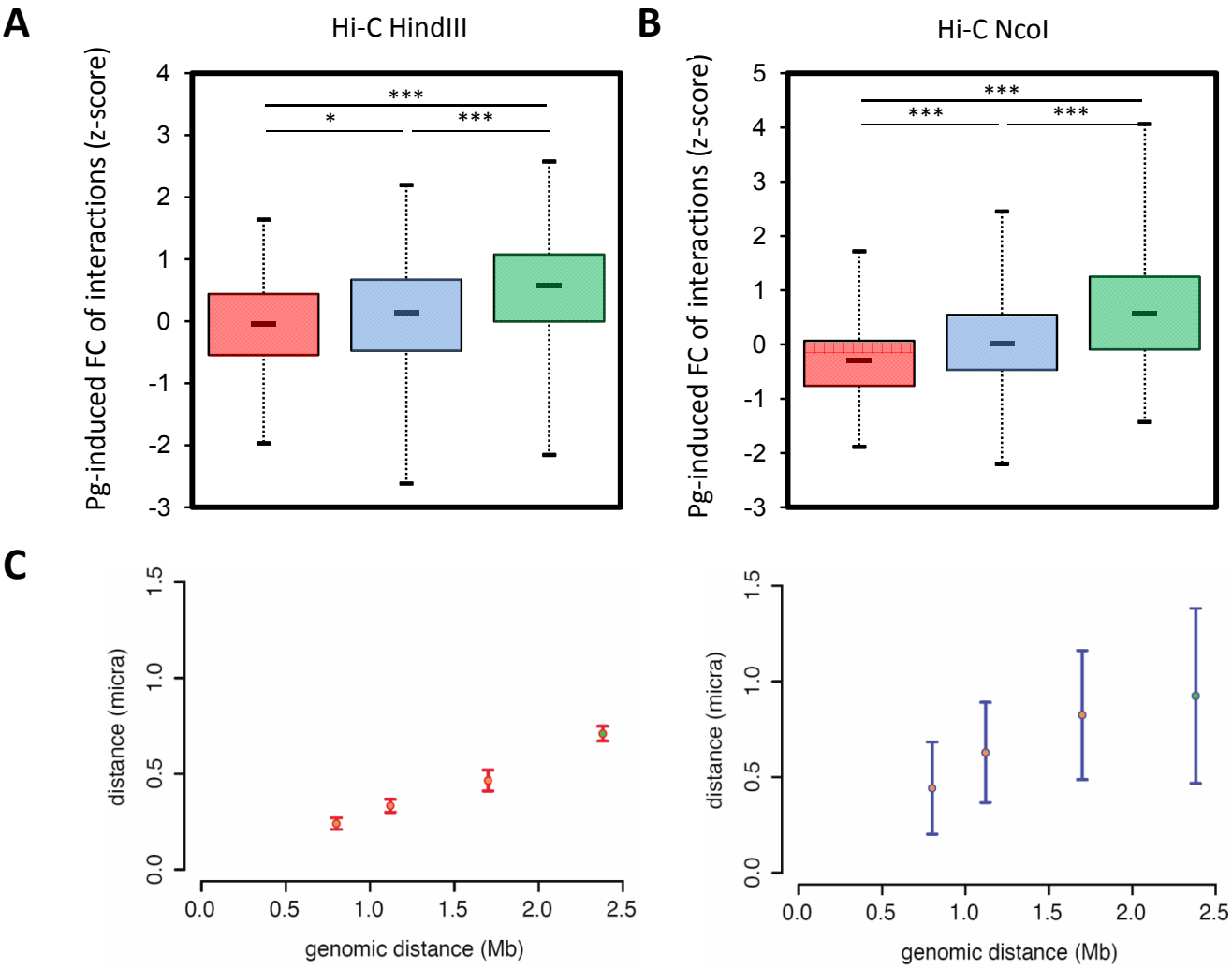
A
Hi-C HindIII
Pg-induced FC of interactions (z-score)
4
3
2
1
0
-1
-2
-3
***
*
***
B
Hi-C NcoI
Pg-induced FC of interactions (z-score)
5
4
3
2
1
0
-1
-2
-3
***
***
***
C
distance (micra)
1.5
1.0
0.5
0.0
0.0
0.5
1.0
1.5
2.0
2.5
genomic distance (Mb)
distance (micra)
1.5
1.0
0.5
0.0
0.0
0.5
1.0
1.5
2.0
2.5
genomic distance (Mb)

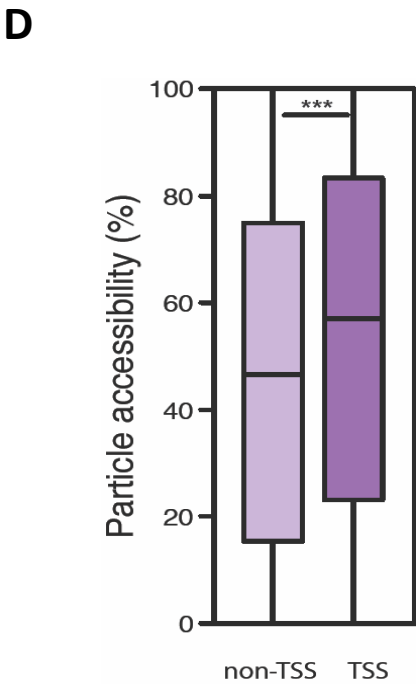
D
Particle accessibility (%)
100
80
60
40
20
0
***
non-TSS
TSS

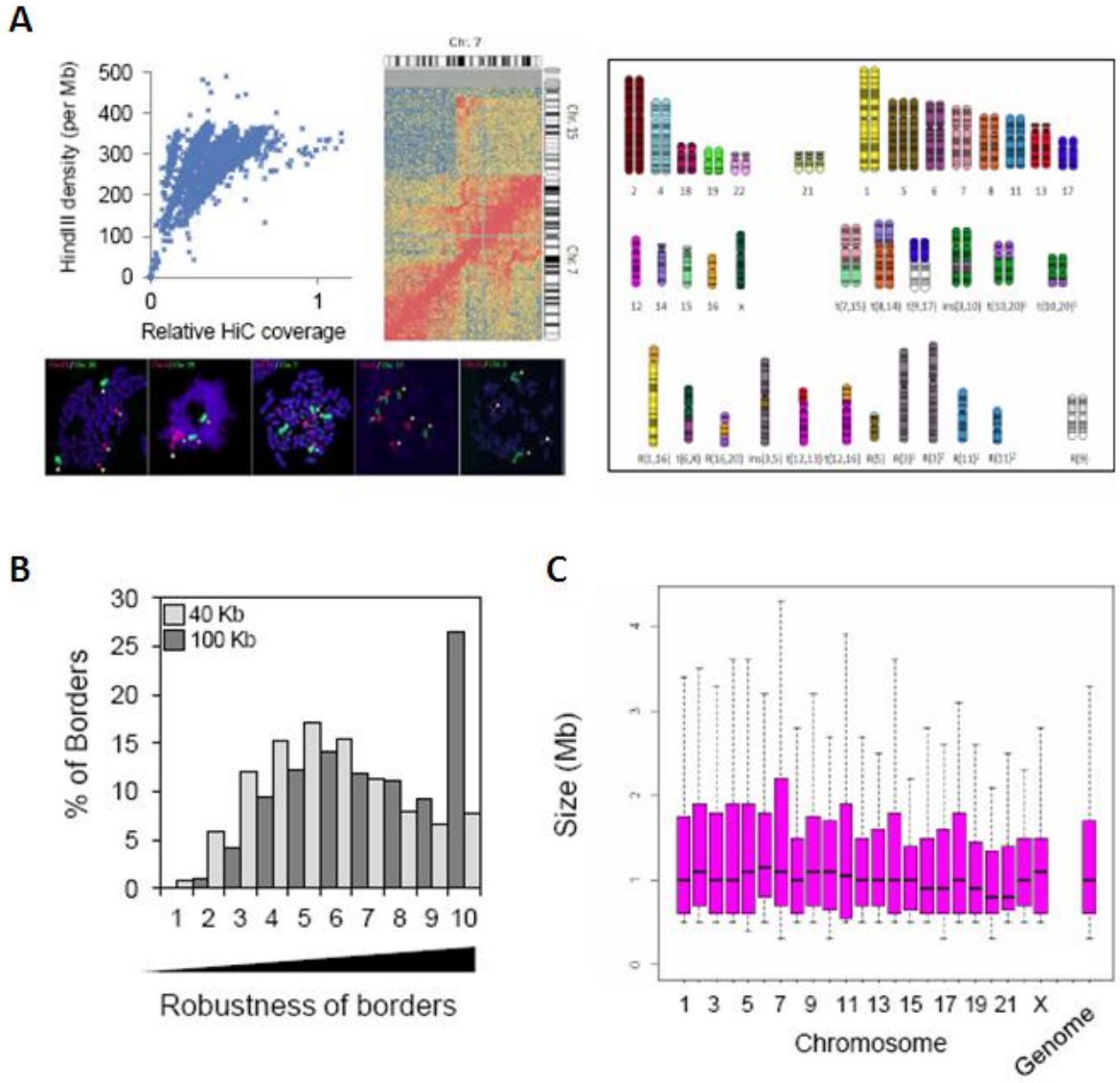

Supplementary Figure 1: T47D genome is organised in TADs.

(A) The linear correlation between number of Hi-C contacts and number of restriction sites is lost due to changes in copy number allowing determining the number of copies of each megabase domains present in T47D genome (top left panel). A snapshot of contact matrix shows an example of translocation breackpoint between the chromosomes 7 and 15 in T47D cells (top middle panel). T47D karyotype deduced from the variations in copy number and translocations events determined as above is represented (right panel). Bottom left panel show examples of 2D-FISH on T47D cells metaphase spreads validating the karyotype and highlighting changes in ploidy, translocation events as well as normal chromosomes. **(B)** Distribution of

boundaries confidence scores for TADs defined at 40 (light grey – n=3027) or 100 Kb (dark grey – n=2031) resolutions. **(C)** Distribution of TAD sizes determined at 100 Kb resolution (N genome=2031).

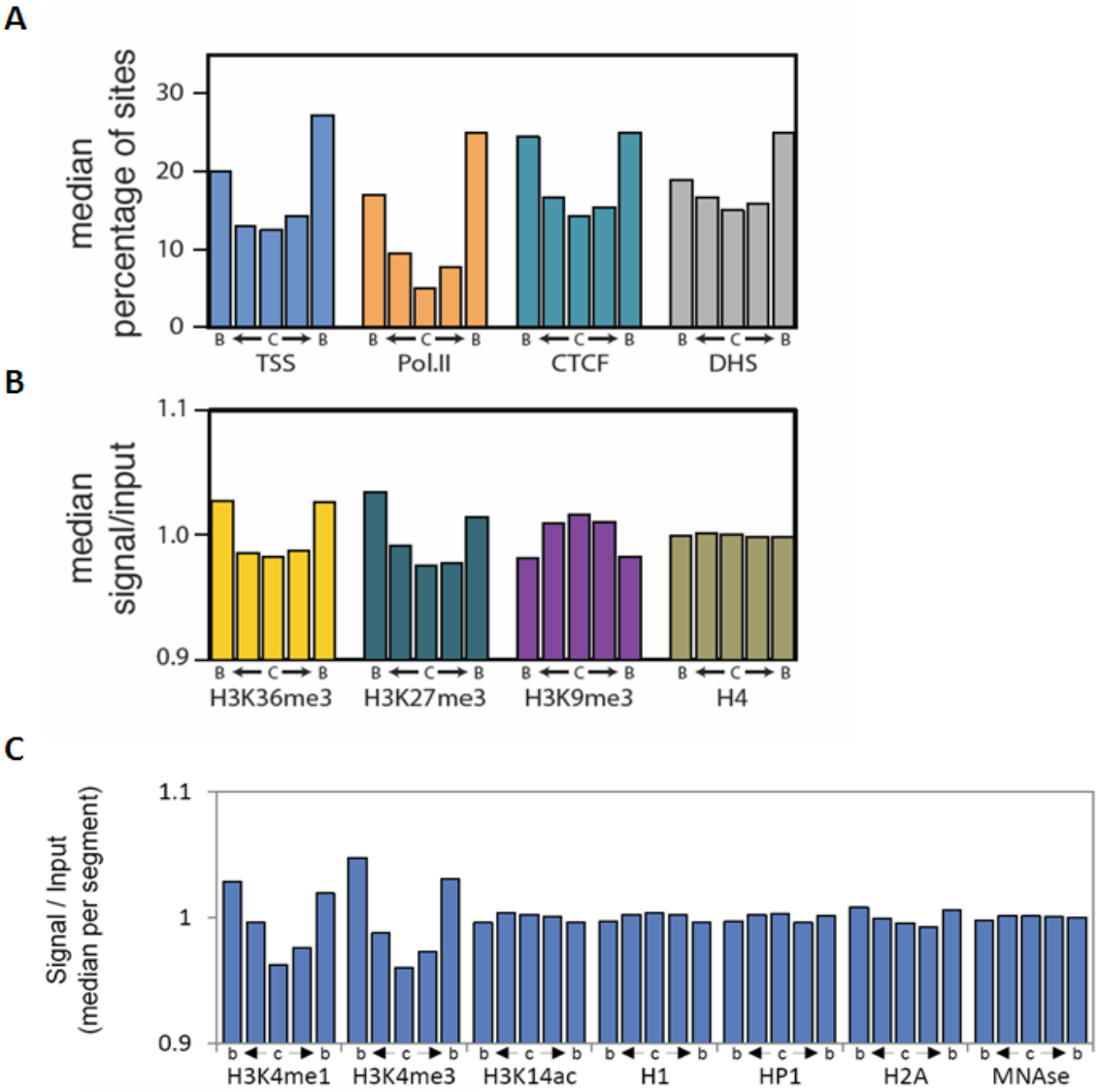

Supplementary Figure 2: Functional characterization of TADs.

TADs were divided into 5 sub-segments of equal size to study the distribution of epigenetic features according a border (b) to center (c) distribution (see Supplementary Methods). **(A)** The median percentage of Transcription Start Sites of protein coding genes (TSS), RNA-Polymerase II (Pol.II), and CTCF binding sites, as well as DNAse I hypersensitive sites (DHS) is shown. **(B)** The histogram represent the median ratio of normalised ChIP-Seq signals over input for H3K36me3, H3K27me3, H3K9me3 and total H4 determined in the TADs 5 sub-segments. **(C)** Normalised ChIP-Seq signals over input ratio were calculated per sub-segment for each TAD for the indicated chromatin components and marks mentioned. Histograms show, for each mark, the median normalised signal/Input observed in the 5 sub-segments for all TADs in the genome.

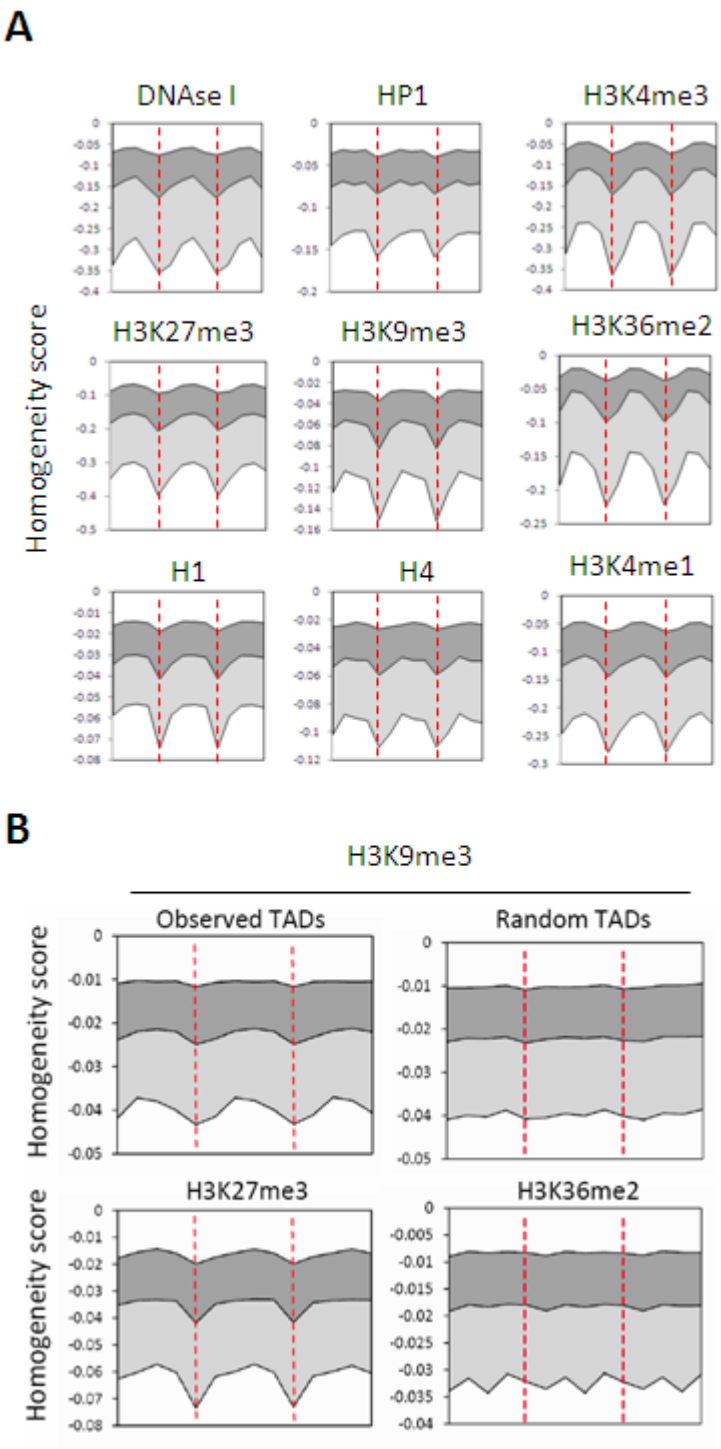

Supplementary Figure 3: TADs are epigenetic domains which chromatin is coordinately modified upon Pg.

(A) Plots show the homogeneity score of the normalised Chip-Seq signal/Input ratio between successive sub-segments (see Supplementary Methods) over 3 consecutive TADs for the chromatin marks and components listed. Lines depict the 25th, 50th and 75th percentiles (from top to bottom respectively) of the scores

computed genome-wide. **(B)** Differences of +Pg/-Pg H3K9me3 Chip-Seq signal between consecutive sub-segments (see Fig. S3 and Supplementary information) over 3 consecutive TADs in the case of observed (*left panel*) or randomized (*right panel*) TADs borders show that transition between Pg induced changes in chromatin state occur preferentially at the TAD boundaries. Similar analysis was performed for other chromatin marks as example H3K27me3 and H3K36me2.

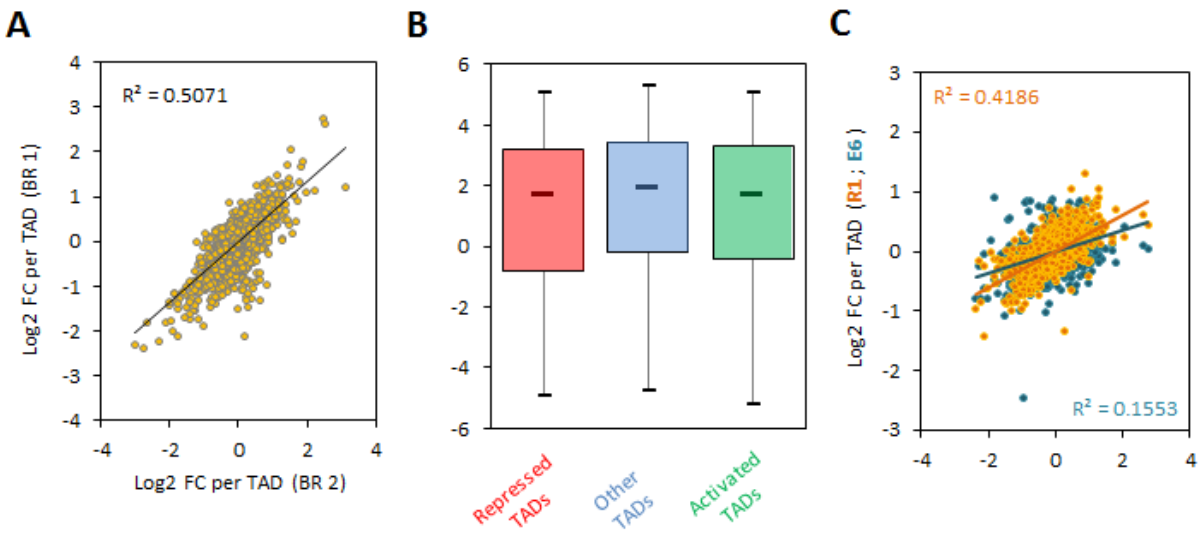

Supplementary Figure 4: Homogeneous and specific response of TADs to steroid hormones.

(A) The ratio of normalised reads after and before 6 hour of treatment with Pg were calculated for each TAD. The scatter plot shows the correlation of response to Pg per TAD obtained in two biological replicates (BR1 and BR2) of RNA-Seq. **(B)** Boxplots show the basal expression levels (RPKM – Log_2) of genes located within the three types of TADs. **(C)** Scatter plot showing the correlation of response per TAD after 6 hours of treatment with Pg (R6) with the changes obtained after 1 hour of Pg induction (R1) or 6 hours of treatment with E2 (E6).

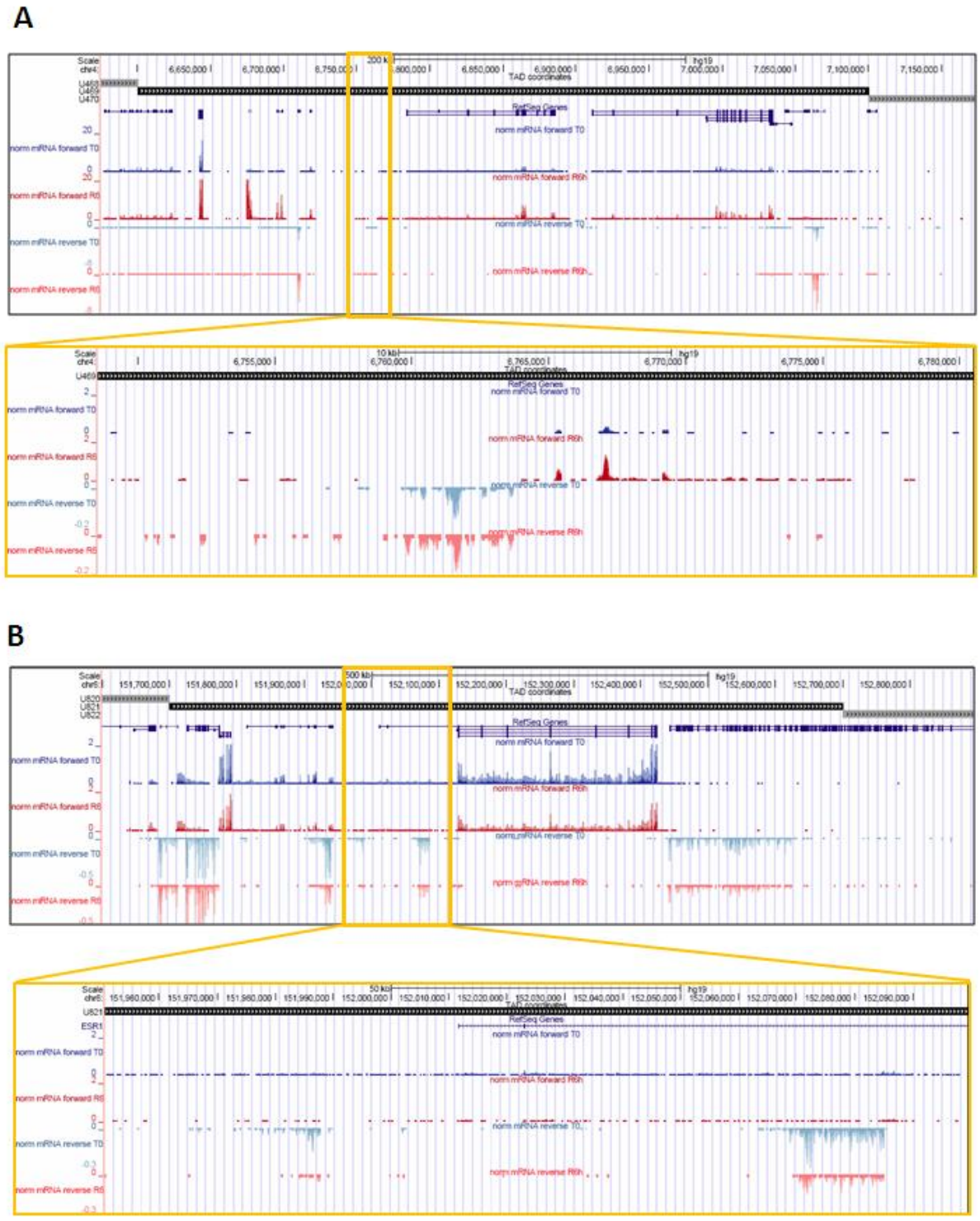

Supplementary Figure 5: TADs respond as unit to the hormone stimulus

(A and B) Genome browser view of RNA-Seq signal within TADs presented in Figure 2E (**(A)** U469; **(B)** U821) highlighting the expression of non-annotated non-coding transcripts which correlate with the hormone induced changes in expression observed for the protein coding genes.

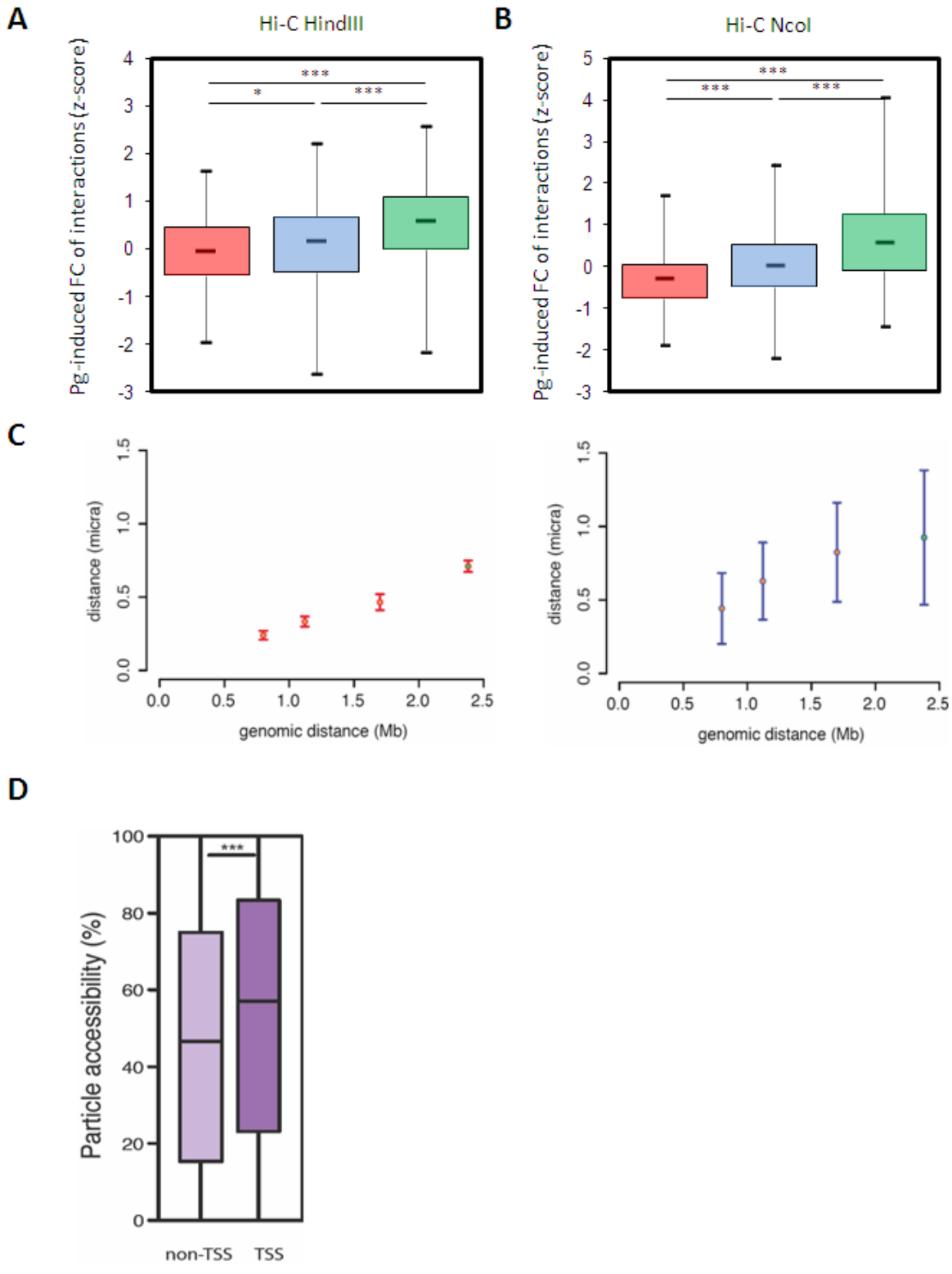

Supplementary Figure 6: Structural changes of TADs.

(A and B) Distributions of the changes of intra-TAD contacts proportions upon Pg treatment (See Extended Experimental Procedures) in the different TAD categories for the two independent datasets obtained with *HindIII* (**A**) or *NcoI* (**B**). Boxplot

whiskers correspond to 5^{st} and 95^{th} percentiles. (***),(**),(*) indicate P < 0.0001, 0.001 and 0.01, respectively (Mann-Whitney test). **(C)** Pair-wise inter-probes 3D distances obtained in the models (left panel) or *in situ* (right panel) were plotted according the genomic distances that separate them. **(D)** Distributions of the accessibility scores calculated from the models for particles containing or not a TSS.